Zinc Thiolate Enables Bright Cu# Deficient Cu#In#S/ZnS Quantum Dots

Zinc Thiolate Enables Bright Cu-deficient Cu-In-S/ZnS Quantum Dots

*Eric C. Hansen, Sophie N. Bertram, Jason J. Yoo, Moungi G. Bawendi**

Department of Chemistry, Massachusetts Institute of Technology, 77 Massachusetts Avenue, Cambridge, Massachusetts 02139, United States

E-mail: mgb@mit.edu

Keywords: Copper Indium Sulfide, Shell Growth

ABSTRACT: Copper Indium Sulfide (CIS) colloidal quantum dots (QDs) are a promising candidate for commercially-viable QD-based optical applications, for example as colloidal photocatalysts or in luminescent solar concentrators (LSCs). CIS QDs with good photoluminescence quantum yields (PLQYs) and tunable emission wavelength via size and composition control have been previously reported. However, developing an understanding and control over the growth of electronically-passivating inorganic shells would enable further improvements of the photophysical properties of CIS QDs. To improve the optical properties of CIS QDs, we focus on the growth of inorganic shells via the popular metal-carboxylate/alkane thiol decomposition reaction. We (1) study the role of Zn-carboxylate and Zn-thiolate on the formation of ZnS shells on Cu-Deficient CIS (CDCIS) QDs, (2) leverage this knowledge to yield >90% PLQY CDCIS/ZnS core/shell QDs, and (3) propose a mechanism for ZnS shells grown from zinc-carboxylate/alkane thiol decomposition.

1. Introduction

Colloidal quantum dots (QDs) are well-suited for low-cost optoelectronic applications, but are limited in commercial translation because the best-performing QDs contain Cadmium (Cd) and/or Lead (Pb). Colloidal Copper Indium Sulfide (CIS) QDs have shown tunable band gaps, large absorption cross-sections, and relatively high photoluminescence quantum yields (PLQYs) while

approaching the performance of Cd- and Pb-containing QDs for LSCs and photocatalysis.[1–10] For further successful translation of CIS QDs as an industrially-viable colloidal material, attention to the synthetic methods that lead to the rational improvement of optical properties is of interest.

Inorganic shells (CdS, ZnS) grown atop CIS QDs are widely reported to improve PLQY by minimizing nonradiative recombination pathways likely associated with surface defects.[6,11–19] However, the growth of inorganic shells that yield high PLQY CIS QDs has been predominantly limited to cation exchange methods by which Zn^{2+} replaces Cu^{+} and In^{3+} to yield a ZnS shell.[7,20,21] In contrast, examples of true ZnS shell growth on CIS QDs require time-intensive methods that achieve a comparatively low PLQY (~50%).[22] Furthermore, successful shell growth methods for II-VI or III-V QD materials do not often translate to CIS due to the propensity of CIS for disproportionation to the binary sulfides (i.e. $Cu_{2-x}S$, In_2S_3) at elevated temperatures.[23–25] An understanding of the underlying chemical manipulations that lead to shell formation is needed to adapt established shell growth methods to the lower temperatures necessary for CIS QDs.[7,21,26,27]

While the metal-carboxylate/alkane thiol decomposition reaction yields growth of high-quality metal sulfide shells on colloidal QDs, this reaction results in cation exchanged shells for CIS QDs.[6] The unique combination of elegance and utility of this reaction lies in its kinetics, which facilitate slow, uniform metal sulfide growth without use of pyrophoric or difficult-to-prepare precursors.[28,29] Furthermore, long-chain alkane thiols are largely inactive sulfur sources which lend themselves to scalable production while showing good bench stability and low volatility. This reaction has been applied to CdSe/CdS core/shell nanoparticles using alkane thiols and Cd-carboxylate at >300°C to produce unity PLQY fluorophores with ideal optical properties at both the ensemble and single-dot level.[28] In contrast to the creation of CIS/ZnS core/shell particles, cation-exchange during growth of CdS on CdSe cores does not impact their optical properties as both core and shell are Cd-based. As a result, the synthesis of effective ZnS shells on CIS QDs is complicated by *A.* the impact of cation

exchange and *B.* the need for lower temperatures, as CIS optical properties are irreversibly lost upon heating beyond 260 °C.

We investigate the mechanism for growth of ZnS shells atop CIS QDs to determine the relevant synthons for growth of different types of ZnS shells (e.g. true shell, cation exchange, or a mixture of the two). We first hypothesize the two relevant Zn^{2+} species for the formation of ZnS in the metal-carboxylate/alkane thiol reaction: Zn-carboxylate and Zn-thiolate. We base this hypothesis on reports using Zn-carboxylate that exclusively produce cation-exchanged ZnS shells unless long reaction times are used, which then lead to true shell formation.[6,22] Long reaction times would favor exchange of Zn-carboxylate with alkane thiol to yield Zn-thiolate, which may then lead to the deposition of ZnS. Thiolate complexes containing Cu^{+} and In^{3+} have been recently revealed as the reactive intermediate in the formation of CIS QDs using thiol-based methods.[30]

2. Results and Discussion

2.1. Role of Zn-carboxylate and Zn-thiolate in ZnS Shell Growth

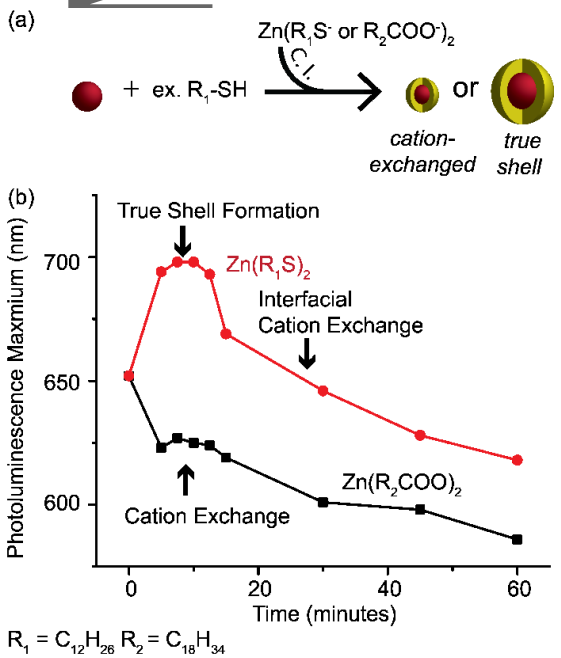

Figure 1. (a) Synthetic scheme comparing the continuous injection (C. I.) of different Zn species into a solution of the same batch of purified CDCIS cores in the presence of excess 1-dodecanethiol. (b) Monitoring of the photoluminescence maximum over time of the reaction described in (a), which shows characteristic continual blue-shift for Zn-carboxylate ($Zn(R_2COO)_2$) associated with cation exchange shell formation by which the CIS core diameter is reduced as the shell grows. In contrast, continuous injection of Zn-thiolate ($Zn(R_1S)_2$) revealed a red-shift, expected for a type-I shell, followed by interfacial alloying that then blue shifts the PL with growth of an alloyed interface that reduces the size of the core CDCIS QD.[21]

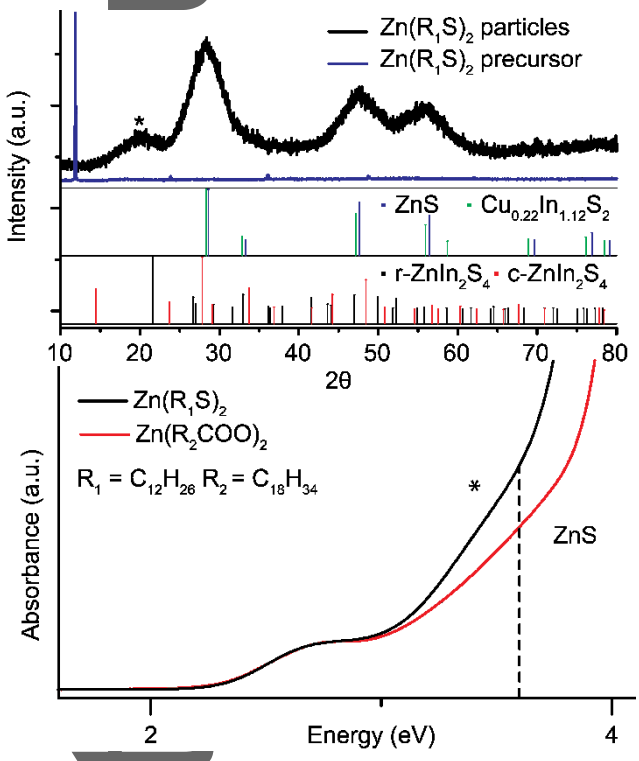

Figure 2. An XRD/UV-Vis comparison of ZnS growth on the same sample of core CDCIS QDs such that the effective core size has been reduced to the same extent (indicated by absorbance onset). Growth using Zn-thiolate ($Zn(R_1S)_2$) results in increased oscillator strength starting at lower energies (marked * in UV-Vis) than the ZnS bulk bandgap, correlates with the emergence of a low angle peak

in XRD (marked * in XRD) ascribed to rhombohedral $ZnIn_2S_4$. XRD of the Zn-thiolate precursor shows that the low angle XRD peak does not arise from excess precursor. Growth using Zn-carboxylate ($Zn(R_2COO)_2$) resulted in decreased core particle size inferred from absorbance onset at lower energies in relation to cores that were too small for XRD analysis. See Figure S1 for the absorbance profile of the core sample. The matched blue-shift of the band edge absorbance position presented between core/shell structures grown with Zn-thiolate or Zn-carboxylate in Figure 2 suggests an equivalent amount of cation-exchange-induced quantum confinement enhancement of the Cu-In-S QD core, enabling direct comparison of optical properties arising from the shell structure surrounding the core. Importantly, the Zn-thiolate core/shell absorbance profile in Figure 2 shows additional optical density at energies too low to arise from ZnS (emphasized with a "*") in comparison to the Zn-carboxylate core/shell, implying that Zn-thiolate leads to the formation of an additional phase, tentatively assigned as a Zn-In-S alloy.

To gain a qualitative understanding of the role of Zn-carboxylate and Zn-thiolate on ZnS shell formation, we performed a shell growth using each species under otherwise identical conditions with the same batch of purified cores, as presented in Figure 1. Zn-carboxylate and Zn-thiolate were prepared directly from diethyl zinc with further chemical analysis confirming their identity (Figure S2-S7). Continuous injection was used to ensure that the desired species was present throughout the course of the reaction. The initial PL red-shift for Zn-thiolate-based shell formation is assigned to the initial growth of a true ZnS shell, followed by interfacial alloying, as has been suggested elsewhere.[21] In contrast, shell formation using Zn-carboxylate exclusively shows a PL blue-shift, as is expected for a cation exchanging shell formation pathway. This experiment demonstrates the qualitative difference in chemical functionality between the two species, suggesting that Zn-thiolate is capable of ZnS deposition to form the expected type-I structure between CIS and ZnS.

Given the qualitative difference in chemical functionality between Zn-thiolate and Zn-carboxylate, we grew a core/shell CDCIS/ZnS structure without CI to compare the precursors. We were able to capture each product such that the absorbance edge was blue-shifted an identical amount by adjusting the temperature of growth for each precursor, meaning that the core of both products had been effectively size-matched to enable ready comparison. Interestingly, we found that shell growth using pure Zn-thiolate resulted in the emergence of a low angle peak in XRD paired with an increase in absorbance (oscillator strength) at energies too low to arise from ZnS, both of which are consistent with the formation of rhombohedral $ZnIn_2S_4$ (Figure 2) (bulk band gap ~2.5 eV). This new low angle peak does not align with the angles of diffraction for the Zn-thiolate precursor.[31] This low angle XRD peak has been previously reported for Zn-Cu-In-S alloy QDs.[31–33] $ZnIn_2S_4$ XRD patterns are known to shift to higher angles with increasing Cu-content, making Reitveld reconstruction impractical since the exact elemental composition of this alloy layer cannot reliably be distinguished from Cu-content in the core QD.[31,32] In total, it is apparent that while Zn-thiolate might be initially capable of ZnS deposition atop CDCIS QDs, *in situ* cation exchange at the particle surface leads to the formation of a Zn-In-S alloy shell rather than yielding pure ZnS.

2.2 Synthesis of High PLQY CDCIS/ZnS QDs.

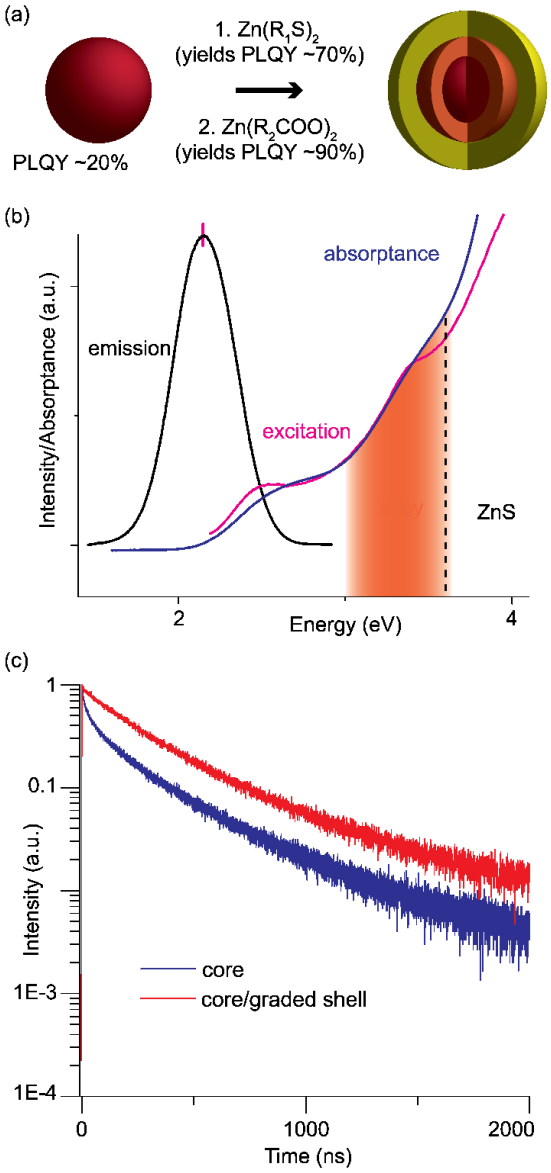

Figure 3. (a) Synthetic scheme for the preparation of high-PLQY CDCIS/ZnS QDs (b) Steady-state optical properties of core/shell CDCIS/ZnS QDs with >90% PLQY show that the shoulder peak associated with the alloyed shell is a part of the excitation trace, indicating that this peak does not arise from a subpopulation within the sample. The dashed line marks the ~3.6 eV bandgap of ZnS while the graded orange region indicates the increased oscillator strength arising from the alloyed region of the shell (c) TRPL traces of the core particles and core/shell particles grown using the step 1/step 2 Zn-thiolate/Zn-carboxylate reaction scheme.

To leverage the ability of Zn-thiolate to produce an alloyed shell, a shell growth method using a two-step procedure was established to prepare a graded composition shell in order to improve the PLQY of the core/shell QDs. A graded shell was designated as the ideal target structure for optimal PLQY as this minimizes interface defects. A thiol-only core synthesis was employed to prevent any undesired cation exchange in the presence of carboxylic acid/carboxylates yielding 1.9 ± 0.3 nm particles (Figure S8 and S9). Our two-step procedure utilizes a first step in which an alloyed shell is deposited using Zn-thiolate (yielding 2.5 ± 0.5 nm particles) followed by a second step to *1.* cation exchange the exterior of the alloy shell and *2.* exchange surface-bound thiolates for carboxylates using Zn-carboxylate (yielding 2.8 ± 0.4 nm particles) to improve PLQY as presented in Figure 3/S10-13. Time-resolved photoluminescence (TRPL) traces indicate that despite removing the fast component of the core lifetime, associated with surface defects, core/graded shell QDs still show a bi-exponential behavior (215 ns (76%) and 639 ns (24%)) (see Figure S14), in agreement with previous reports of CDCIS/ZnS QDs.[4] To illustrate the utility of a chemically-controlled shell growth, relative to an externally-controlled (e.g. continuous or rapid injection) shell growth, we scaled our reaction by a factor of 10 and found that the optical properties translated with minimal deviation (Figure S15). Improvement of PLQY by exchange of surface-bound thiolates for carboxylates is supported by previous reports showing high-thiolate capping can lead to electron traps.[34] While our work results in some of the best photophysical properties for CIS to date, we note the need for continued optimization of the PLQY for applications that require true unity PLQY fluorophores for optimal performance.

2.3 Manipulation of Interfacial Alloying.

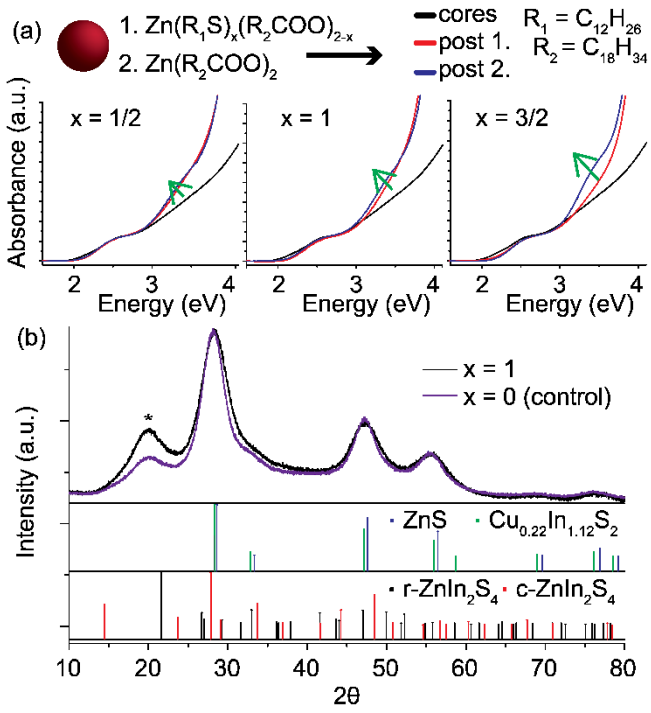

Figure 4. (a) Comparative UV-Vis spectra of purified CDCIS/ZnS QDs prepared with differing ratios of carboxylate:thiolate (The "x" value presented in the figure is in reference to the "x" value in $Zn(R_1S)_x(R_2COO)_{2-x}$, such that a larger x corresponds to a greater thiolate character) used in the first step of shell growth, revealing that the shoulder peak between ~3 and ~3.5 eV scales with increasing thiolate character in the first shell precursor. (b) XRD of high PLQY CDCIS/ZnS QDs synthesized from 1:1 carboxylate:thiolate Zn precursor in the first step compared to a control CDCIS/ZnS QD grown with Zn-carboxylate as both the first and second shell precursor. An increase in the lower angle peak (marked with a "*") is indicative of the formation of rhombohedral $ZnIn_2S_4$, with all other reflections being consistent with cubic $Cu_{0.22}In_{1.12}S_2$ and ZnS.

To more fully investigate the chemistry and resultant photophysical properties involved in our high-PLQY CDCIS/ZnS synthesis, we modulated the ratio of thiolate to carboxylate in the first reaction step of the shell growth. We controlled the ratio of Zn-thiolate species, the hypothesized active species for ZnS deposition, relative to Zn-carboxylate species, the hypothesized inactive species, by

using a mixed species thiolate/carboxylate Zn precursor (see SI), summarized in Figure 4. A shoulder peak in the UV-Vis spectrum increases with greater thiolate character, which is correlated with the formation of a rhombohedral $ZnIn_2S_4$ alloy phase by XRD as mentioned earlier. We suggest that this alloyed phase exists as a layer between the CDCIS core and ZnS shell. The apparent increase in oscillator strength of the alloy peak from step 1 to step 2 may arise from filling crystal vacancies with Zn^{2+} to yield $ZnIn_2S_4$. We conclude from this experiment that the thiolate:carboxylate ratio used in the first shell growth step impacts the extent of interfacial alloying.

2.4 Chemical Mechanism of ZnS Shell Growth

After assessing optical characteristics as a function of the ratio of thiolate:carboxylate, we chemically characterized the reaction mixtures of the same experiment (Figure S16-S18). NMR reveals that the decomposition of mixed character Zn-thiolate/carboxylate complexes with CDCIS cores exclusively yields thioether (R_1S-$R_{1\ or\ 2}$) (see Scheme 1a) without evidence of ester ($R_2COOR_{1\ or\ 2}$) formation (see Scheme 1b). Ester formation would be the signature of direct reaction of Zn-carboxylate with alkane thiol to yield ZnS (see Scheme 1b), which is not observed and is therefore an inefficient reaction pathway. The PL red-shift observed with Zn-thiolate in Figure 1 paired with the lack of ester formation when using a mixed Zn-thiolate/carboxylate precursor in Figure S19 provides support for our hypothesis that Zn-thiolate is the active species of ZnS formation while Zn-carboxylate is inactive.

Proposed Routes for Direct Synthesis of a ZnS shell

(a) $Zn(R_1S)_2 \rightarrow ZnS + R_1SR_1$

(b) $Zn(R_2COO)_2 + R_1SH \rightarrow ZnS + R_2COOR_1 + R_2COOH$

Scheme 1. Direct ZnS shell forming reactions using (a) Zn-thiolate and (b) Zn-carboxylate. The chemical signature of reaction (a) is the formation of thioether (R_1SR_1) while reaction (b) is marked by the formation of ester (R_2COOR_1). $R_1 = C_{12}H_{16}$, $R_2 = C_{18}H_{34}$

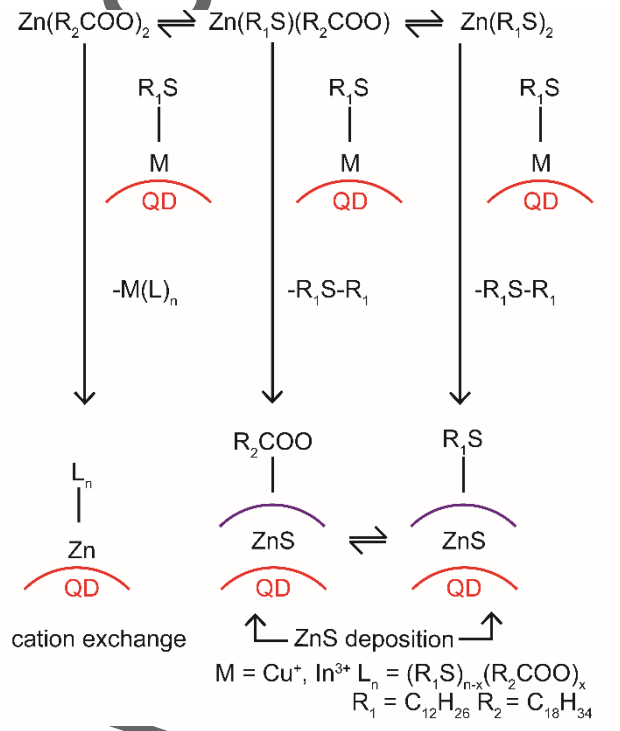

Figure 5. Proposed reaction diagram for the cation exchange versus true shell growth of ZnS shells on thiolate-capped CIS cores in which Zn-carboxylate exchanges surface-bound metal ions to yield a cation exchanged shell while Zn-thiolate decomposes to form a ZnS layer with associated formation of a thioether (R-SR). We note that $Zn(R_1S)(R_2COO)$ refers to a hypothesized molecularly-defined intermediate between Zn-carboxylate and Zn-thiolate, while our experiments regarding interfacial alloying used a mixture of Zn-species with a known thiolate:carboxylate ratio, but without molecular definition. $M(L)_n$ refers to the various complexes that could form upon loss of M^{n+} (i.e. Cu^+, In^{3+}) from the QD surface.

We combine our chemical observations regarding the formation of ZnS shells on CDCIS/ZnS QDs in Figure 5 to provide a basic reaction mechanism for ZnS formation. First, we propose three Zn-containing species in equilibrium due to ligand exchange of Zn-carboxylate with excess free thiol: Zn-carboxylate, mixed character Zn-carboxylate/thiolate, and Zn-thiolate. From our observation of a spectral blueshift without any initial redshift when forming ZnS shells using Zn-carboxylate in Figure 1 and the lack of ester formation as presented in Scheme 1/Figure S19, we suggest Zn-carboxylate leads to cation exchange of the surface without direct formation of ZnS. This Zn-carboxylate-induced cation exchange results in surface capping with thiolate or carboxylate. From our observation of spectral redshift in Figure 1 and the observed formation of thioether in Figure S16-S18, we suggest that Zn-thiolate leads to the deposition of ZnS, which then forms a $ZnIn_2S_4$ alloy by interfacial alloying. Mixed carboxylate/thiolate precursors with increasing thiolate character led to increasing alloy formation as seen in Figure 2-4. The correlation of thiolate character to alloy formation along with the lack of ester formation observed in Figure S19 suggests that only the zinc thiolate part of mixed character Zn-carboxylate/thiolate species leads to the formation of ZnS. The lack of ester formation suggests that even if Zn-carboxylate is capable of producing ZnS (Scheme 1b), ZnS formation from Zn-thiolate (Scheme 1a) is markedly faster. In describing the roles of the various synthons relevant to the formation of ZnS shells at temperatures <300 °C, we hope that this analysis will enable rational precursor selection for ZnS-shelled nanostructures on temperature-sensitive colloidal materials.

3. Conclusion

In total, we propose a mechanistic understanding of the role of Zn-thiolate and Zn-carboxylate in the synthesis of ZnS shells on colloidal nanocrystals and use our insights to synthesize high PLQY CDCIS QDs. Our analysis indicates that Zn-thiolate is the active species for ZnS formation, which enables PLQY improvements. These results indicate that the ratio between Zn-carboxylate to Zn-

thiolate is a deciding factor in the identity of ZnS-based shells on CDCIS QDs. By manipulating the amount of active shell precursor present in the reaction (instead of relying on *in situ* formation), we extend applicability of metal sulfide shell formation by metal carboxylate/alkane thiol decomposition to lower temperatures/shorter reaction times, appropriate for thermally unstable QD materials. We hope that these results can provide (1) a rational framework for the further application of ZnS inorganic shells on colloidal QDs, (2) an example of a high-PLQY QD material that is scalable and suitable for applications, and (3) a description of a potential mechanism in the synthesis of ZnS shell nanostructures.

4. Experimental Section

4.1 Chemicals and Materials

All chemicals were acquired and used without further purification. 1-dodecanethiol (Alfa Aesar, 98%), trioctylphosphine (Sigma-Aldrich, 97%), 1-octadecene (Acros Organics, 90%), Oleic acid (for Figure 1 experiment: Sigma Aldrich >99%; otherwise: Alfa Aesar, 90%), Indium (III) Acetate (Alfa Aesar, 99.99% metals basis), Copper (I) Iodide (Aldrich, 98%), Zinc Acetate Dihydrate (Sigma-Aldrich, >99%), Diethyl Zinc (Beantown Chemicals, 96%). *Caution: Diethyl zinc is extremely pyrophoric and must be handled under an inert atmosphere.*

4.2 Synthetic Methods

Stock Core Synthesis (Figure 1 and 2):

First, CDCIS core QDs were prepared by a modified literature preparation.[6] 16 mmol Indium (III) acetate, 4 mmol Copper (I) iodide, 10 mL 1-dodecanethiol, 8 mL oleylamine, 8 mL oleic acid, and 100 mL 1-octadecene were heated to 120°C under vacuum for 10 minutes before heating to 210°C under

nitrogen. After 1 hour at this temperature, the reaction was cooled to room temperature before crashing with acetone and redispersing the resulting pellet in 100 mL 1-octadecene.

Continuous Injection Experiment (Figure 1):

For the Zn-thiolate variant, 4 mmol diethyl zinc was added to 6 mL of trioctylphosphine in a 20 mL vial in a nitrogen-filled glovebox. In a separate 20 mL vial, 8 mmol 1-dodecanethiol was added to 4 mL trioctylphosphine. The 1-dodecanethiol solution was added dropwise to the diethyl zinc solution over the course of several minutes at room temperature while rapidly stirring. The reaction was stirred at room temperature for 30 minutes to yield a colorless solution that was used without further purification. For the Zn-carboxylate variant, the same procedure was followed, with oleic acid substituted for 1-dodecanethiol.

In a 3-neck 100 mL round bottom flask, 2 mL of purified cores described in "*Stock Core Synthesis (Figure 1 and 2)*" were added to 6 mL 1-octadecene and 2 mL 1-dodecanethiol. This solution was briefly degassed at 100°C before heating to 240°C, at which point $Zn(R_1S)_2$ or $Zn(R_2COO)_2$ were injected at a rate of 0.5 mL/hour. Once precursor injection began, solution temperature was increased to 250°C.

Cation Exchange versus Zn-thiolate Experiment (Figure 2):

For the $Zn(R_2COO)_2$ cation exchange: In a 3-neck 25 mL round bottom flask, 5 mL 1-octadecene, 8 mmol oleic acid, and 4 mmol zinc acetate dihydrate were heated to 100°C for 1 hour under vacuum. Next, added 8 mmol 1-dodecanethiol and 2 mL of the CDCIS QDs described in "*Stock Core Synthesis (Figure 1 and 2)*" and degassed for 5 more minutes. Next, the reaction was rapidly heated to 200°C under N_2, where it was held for 1 hour before cooling to room temperature. The mixture was then crashed three times with acetone and re-dispersed in chloroform.

For the $Zn(R_1S)_2$ comparison: In a 3-neck 25 mL round bottom flask, 5 mL 1-octadecene, 8 mmol 1-dodecanethiol, and 4 mmol zinc acetate dihydrate at 100°C for 1 hour under vacuum. Next, added 2 mL of the CDCIS QDs described in *"Continuous Injection Experiment (Figure 1)"* and degassed for 5 more minutes. Next, the reaction was rapidly heated to 240°C under N_2, where it was held for 1 hour before cooling to room temperature. The mixture was then crashed three times with acetone and re-dispersed in chloroform.

Synthesis of High-PLQY CDCIS/ZnS QDs (Figure 3):

In a 3-neck 25 mL round bottom flask, 0.5 mmol Indium (III) acetate, 0.125 mmol Copper (I) iodide, and 5 mL 1-dodecanethiol were heated to 100°C under vacuum for 30 minutes. The solution was then rapidly heated to 230°C under nitrogen (usually in 6 minutes), where it was maintained for 5 minutes before rapidly cooling by nitrogen stream to yield a bright red solution of CDCIS core QDs.

Meanwhile, in a 3-neck 100 mL round bottom flask, 8 mL 1-octadecene, 4 mmol Zinc (II) acetate dihydrate, and 8 mmol 1-dodecanethiol were heated to 100°C under vacuum for 1 hour to yield a gel-like solid, which was used without further purification.

The core reaction mixture was syringe transferred to the freshly-prepared $Zn(R_1S)_2$ solution. This mixture was then rapidly heated to 240°C under nitrogen, becoming homogeneous around 190°C. After 1 hour at 240°C, the reaction was cooled ambiently to room temperature to yield core/shell CDCIS/ZnS QDs.

Meanwhile, in a 3-neck 100 mL round bottom flask, 8 mL 1-octadecene, 4 mmol Zinc (II) acetate dihydrate, and 8 mmol oleic acid was heated to 100°C under vacuum for 1 hour to yield a colorless, viscous solution, which was used without further purification.

Next, $Zn(R_2COO)_2$ was transferred by syringe to the CDCIS/ZnS QDs reaction mixture described in the preceding paragraph. This mixture was then heated to 240°C under nitrogen, where it was held for 1 hour before allowing to cool ambiently to room temperature. 5 mL of $CHCl_3$ was added to the reaction mixture to homogenize the solution before crashing three times with acetone and re-dispersing in chloroform.

To scale this reaction, cores were reacted for 13 minutes rather than 5 minutes while all parts were repeated identically at ten times the scale.

Mixed Character Precursor Reaction (Figure 4):

First, prepared cores as described in "Synthesis of High-PLQY CDCIS/ZnS QDs" without precipitation.

Next, In a 1-neck 50 mL round bottom flask, 2 mL 1-octadecene, 0.8 mmol Zinc (II) acetate dihydrate, x*0.8 mmol 1-dodecanethiol (e.g. 0.8 mmol for x = 1), and (2-x)*0.8 mmol oleic acid were heated to 100°C for 1 hour under vacuum and used without further purification before cooling to room temperature.

1 mL of core QD solution (1/5 of the reaction mixture) was added to each flask containing mixed character Zn precursor before heating (by oil bath) the reaction mixture to 240°C under nitrogen. Note that all three variants of the shell growth reaction (x = 1/2, 1, 3/2) were performed simultaneously. After one hour, the reaction was cooled to room temperature and 0.8 mmol of $Zn(R_2COO)_2$ solution was added to each reaction mixture. The solution was heated under nitrogen to 240°C, where it was held for one hour before being cooled to room temperature. Each reaction mixture was then crashed three times with acetone and dispersed in hexanes for characterization.

Supporting Information

Supporting Information is available from the Wiley Online Library or from the author.

Acknowledgements

This work was supported in part by the Department of Energy (DOE), Office of Basic Energy Sciences, Division of Materials Sciences and Engineering (Award Number DE-FG02-07ER46454). E.C.H. had Government support under and awarded by the Department of Defense, Air Force Office of Scientific Research, National Defense Science and Engineering Graduate (NDSEG) Fellowship, 32 CFR 168a. S.N.B. (measurement of fluorescence lifetimes) was funded by the Department of Energy (DOE), Office of Basic Energy Sciences, Division of Materials Sciences and Engineering (Award Number DE-FG02-07ER46454) and through a National Science Foundation Graduate Fellowship. J.J.Y. (measurement of X-ray diffractions spectra) was funded by the National Aeronautics and Space Administration (NASA) grant NNX16AM70H. This work made use of the Shared Experimental Facilities supported in part by the MRSEC Program of the National Science Foundation under Grant DMR-1419807. E.C.H. acknowledges Y. Zhang for assistance with TEM.

Received: ((will be filled in by the editorial staff))
Revised: ((will be filled in by the editorial staff))
Published online: ((will be filled in by the editorial staff))

References

[1] M. R. Bergren, N. S. Makarov, K. Ramasamy, A. Jackson, R. Guglielmetti, H. McDaniel, *ACS Energy Lett.* **2018**, 520.

[2] I. Coropceanu, M. G. Bawendi, *Nano Lett.* **2014**, *14*, 4097.

[3] H. Zhong, Ḱ. S. S. Lo, T. Mirkovic, Y. Li, Y. Ding, Y. Li, G. D. Scholes, **2010**, *4*, 5253.

[4] T. J. Daou, P. Reiss, N. Q. Liem, L. Li, I. Texier, T. T. Kim Chi, *Chem. Mater.* **2009**, *21*, 2422.

[5] N. Lequeux, T. Pons, B. Dubertret, F. Marchal, F. Guillemin, L. Bezdetnaya, E. Cassette, E. Pic, *ACS Nano* **2010**, *4*, 2531.

[6] L. Li, A. Pandey, D. J. Werder, B. P. Khanal, M. Pietryga, V. I. Klimov, *J. Am. Chem. Soc.* **2011**, *133*, 1176.

[7] L. De Trizio, M. Prato, A. Genovese, A. Casu, M. Povia, R. Simonutti, M. J. P. Alcocer, C. D. Andrea, F. Tassone, L. Manna, *Chem. Mater.* **2012**, *24*, 2400.

[8] Z. Zhang, K. Edme, S. Lian, E. A. Weiss, *J. Am. Chem. Soc.* **2017**, *139*, 4246.

[9] S. Lian, M. S. Kodaimati, E. A. Weiss, *ACS Nano* **2018**, *12*, 568.

[10] S. Lian, M. S. Kodaimati, D. S. Dolzhnikov, R. Calzada, E. A. Weiss, *J. Am. Chem. Soc.* **2017**, *139*, 8931.

[11] P. M. Allen, M. G. Bawendi, *J. Am. Chem. Soc.* **2008**, *130*, 9240.

[12] A. C. Berends, F. T. Rabouw, F. C. M. Spoor, E. Bladt, F. C. Grozema, A. J. Houtepen, L. D. A. Siebbeles, C. De Mello Donegá, *J. Phys. Chem. Lett.* **2016**, *7*, 3503.

[13] Y.-K. Kim, S.-H. Ahn, K. Chung, Y.-S. Cho, C.-J. Choi, *J. Mater. Chem.* **2012**, *22*, 1516.

[14] V. K. Komarala, C. Xie, Y. Wang, J. Xu, M. Xiao, *J. Appl. Phys.* **2012**, *111*, 124314.

[15] J. Seo, S. Raut, M. Abdel-Fattah, Q. Rice, B. Tabibi, R. Rich, R. Fudala, I. Gryczynski, Z. Gryczynski, W. J. Kim, S. Jung, R. Hyun, *J. Appl. Phys.* **2013**, *114*, 1.

[16] W. Zhang, Q. Lou, W. Ji, J. Zhao, X. Zhong, *Chem. Mater.* **2014**, *26*, 1204.

[17] D.-E. Nam, W.-S. Song, H. Yang, *J. Mater. Chem.* **2011**, *21*, 18220.

[18] S. H. Park, A. Hong, J. H. Kim, H. Yang, K. Lee, H. S. Jang, *ACS Appl. Mater. Interfaces* **2015**, *7*, 6764.

[19] S.-Y. Yoon, J.-H. Kim, E.-P. Jang, S.-H. Lee, D.-Y. Jo, Y. Kim, Y. R. Do, H. Yang, *Chem. Mater.* **2019**, *31*, 2627.

[20] J. Park, S.-W. Kim, *J. Mater. Chem.* **2011**, *21*, 3745.

[21] A. C. Berends, W. Van Der Stam, J. P. Hofmann, E. Bladt, J. D. Meeldijk, S. Bals, C. De Mello Donega, *Chem. Mater.* **2018**, *30*, 2400.

[22] H. Zang, H. Li, N. S. Makarov, K. A. Velizhanin, K. Wu, Y. S. Park, V. I. Klimov, *Nano Lett.* **2017**, *17*, 1787.

[23] R. Xie, M. Rutherford, X. Peng, *J. Am. Chem. Soc.* **2009**, *131*, 5691.

[24] W. P. Lim, C. T. Wong, S. L. Ang, H. Y. Low, W. S. Chin, *Chem. Mater.* **2006**, *18*, 6170.

[25] A. E. Saunders, M. B. Sigman, F. Lee, B. A. Korgel, T. Hanrath, A. Ghezelbash, *J. Am. Chem. Soc.* **2003**, *125*, 16050.

[26] A. Moser, M. Yarema, W. M. M. Lin, O. Yarema, N. Yazdani, V. Wood, *J. Phys. Chem. C* **2017**, *121*, 24345.

[27] B. Chen, H. Zhong, W. Zhang, Z. Tan, Y. Li, C. Yu, T. Zhai, Y. Bando, S. Yang, B. Zou, *Adv. Funct. Mater.* **2012**, *22*, 2081.

[28] O. Chen, J. Zhao, V. P. Chauhan, J. Cui, C. Wong, D. K. Harris, H. Wei, H. S. Han, D. Fukumura,

R. K. Jain, M. G. Bawendi, *Nat. Mater.* **2013**, *12*, 445.

[29] Z. Wang, X. Zhang, W. Xin, D. Yao, Y. Liu, L. Zhang, W. Liu, W. Zhang, W. Zheng, B. Yang, H. Zhang, *Chem. Mater.* **2018**, *30*, 8939.

[30] M. Gromova, A. Lefrancois, L. Vaure, F. Agnese, D. Aldakov, A. Maurice, D. Djurado, C. Lebrun, A. de Geyer, T. U. . Schulli, S. Pouget, P. Reiss, *J. Am. Chem. Soc.* **2017**, *2*, 1076.

[31] S. Shen, L. Zhao, Z. Zhou, L. Guo, *J. Phys. Chem. C* **2008**, *112*, 16148.

[32] X. Wang, Z. Liang, X. Xu, N. Wang, J. Fang, J. Wang, G. Xu, *J. Alloys Compd.* **2015**, *640*, 134.

[33] Z. Guan, J. Pan, Q. Li, G. Li, J. Yang, *ACS Sustain. Chem. Eng.* **2019**, *7*, 7736.

[34] S. Jeong, J. Nanda, J. A. Hollingsworth, M. Achermann, V. I. Klimov, S. Ivanov, *J. Am. Chem. Soc.* **2007**, *127*, 10126.

Keyword: Quantum Dots

Title: Zinc Thiolate Enables Bright Cu-deficient Cu-In-S/ZnS Quantum Dots

Authors: Eric C. Hansen, Sophie N. Bertram, Jason J. Yoo, Moungi G. Bawendi*

TOC FIGURE:

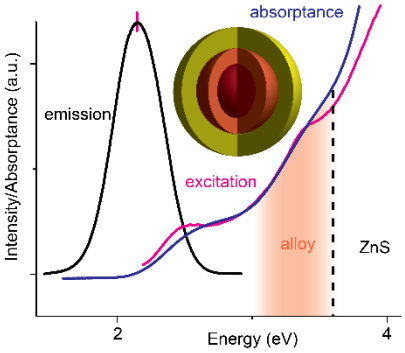

TOC Text:

Zn-thiolate ($Zn(RS)_2$) favors formation of a Zn-In-S alloy when used to grow a ZnS shell on Cu-In-S QDs. Utilizing Zn-thiolate, a graded shell was grown on Cu-In-S QDs to realize >90% record quantum yields.